Additive Manufacturing: Metallurgy, Cut Analysis & Porosity

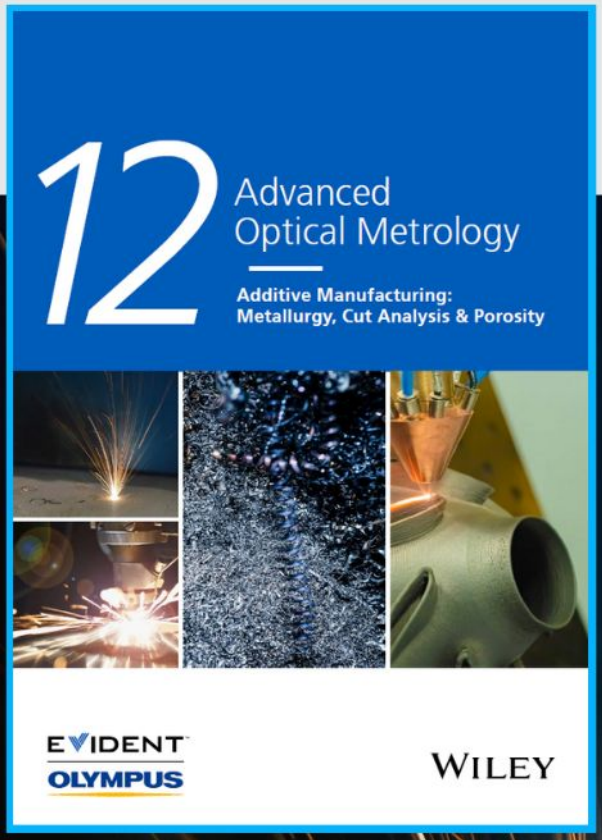

The latest eBook from Advanced Optical Metrology. Download for free.

In industry, sector after sector is moving away from conventional production methods to additive manufacturing, a technology that has been recommended for substantial research investment.

Download the latest eBook to read about the applications, trends, opportunities, and challenges around this process, and how it has been adapted to different industrial sectors.

EVIDENT
OLYMPUS

WILEY

ADVANCED FUNCTIONAL MATERIALS
www.afm-journal.de

Multiple Shape Manipulation of Liquid Crystal Polymers Containing Diels-Alder Network

*Xin Huang, Lang Qin, Jinlei Wang, Xiao Zhang, Bo Peng, and Yanlei Yu**

Multiple shape manipulation of soft materials, including reversible deformation, shape memory effect, and shape remolding, are highly desirable in morphing structures and soft actuators. Although liquid crystal network (LCN) is a promising candidate for realizing anisotropic reversible deformation, developing LCN with multiple shape manipulation remains a multitude of challenges, which is limited to the regulation of mesogens alignment and network topological rearrangement. Here, multiple shape manipulation is demonstrated by a newly designed LCN containing azobenzene moieties and a dynamic Diels-Alder (DA) network. Photodeformation of the LCN is attributed to the ordered lamellar structure of mesogens formed by annealing-induced self-assembly. Light-induced shape memory effect leads to reprogrammable shape changes due to the light-switchable glass transition temperature of the azobenzene-containing LCN. Moreover, the dynamic equilibrium of the DA network endows the LCN with liquid state remoldability and solid state plasticity, which further contributes to diverse 3D geometric shapes in shape remolding. Such LCN exhibiting flexible deformation and remolding properties provides a new photoresponsive block for the fabrication of soft actuators.

1. Introduction

Multiple shape manipulation, including reversible deformation, shape memory effect, and shape remolding, in response to external stimuli, such as heat,[1] light,[2–4] or magnetic field,[5] is highly desirable in the fields of morphing structures, soft actuators, and robotics. A wide range of novel materials have been developed to date, among which liquid crystal network (LCN) is an ideal candidate to realize reversible deformation such as contraction,[6,7] bending,[8–12] and twisting.[13] The key to enable LCN deformation is the alignment change of mesogens induced by thermal (photothermal)[14] or photochemical LC-isotropic phase transition.[15] In the past decades, various alignment techniques, including mechanical stretching/shear,[16–18] topological/chemical surface interactions,[19–21] and remote fields (light,[22] magnetic,[23] or electric[24]), have been reported to obtain the diverse alignment of mesogens in LCN actuators, which demonstrate reversible actuation, such as creeping,[25] oscillation,[26] rotation,[27] etc. However, the obtained alignment of mesogens is typically fixed by traditional cross-linking network, whose permanent nature thus determines that the shape of the LCN actuators cannot be remolded.

A particularly attractive approach to realize shape remolding is to incorporate dynamic covalent bonds into the LCN. Transesterification,[18,28–30] disulfide,[31] and allyl sulfide groups[32] are frequently used to construct dynamic network, which are triggered by high temperature above the topology-freezing transition temperature (T_v) of the LCN. Such dynamic network can undergo topological rearrangement at temperature above T_v by taking advantage of its dynamic equilibrium and consequently give rise to shape remolding of the LCN. If the T_v is higher than isotropic temperature (T_i) of the LCN, the alignment of the mesogens will be disturbed, leading to the failure of reversible deformation. Therefore, Diels-Alder (DA) bonds have attracted increasing attention because of the mild T_v (typically ranging from 60 to 100 °C[33]) above which the alignment of the mesogens remains an ordered state while diverse 3D geometric shapes of the LCN actuators are reprogrammed by the shape remolding. Zhao et al. reported a main-chain LCN containing the DA network, which allows for the formation of solid 3D actuators, strip walker and wheel-capable light-driven locomotion, realizing the combination of reversible deformation and shape remolding.[34]

In addition, the LCN possesses shape memory effect due to the physical phase transition (e.g., glass transition) to program temporary shape and the network to fix the permanent shape.[35] Recently, we introduced azobenzene moieties serving as a light-switchable transition unit into the dynamic LCN with ester bonds, demonstrating shape remolding and light-induced shape memory performance.[36] The *trans-cis* photoisomerization of azobenzene moieties regulate the glass transition temperature (T_g) of the LCN above or below the room temperature (RT), and subsequently induces the reversible transition between glassy state (*trans* form, low chain mobility) and rubbery state (*cis* form, high chain mobility). The LCN at the rubbery state ($T_{g\text{-cis}}$ < RT) is programmed into a temporary shape that is then fixed by frozen segments at the glass state ($T_{g\text{-trans}}$ > RT). Shape recovery of the permanent shape is triggered by the irradiation

X. Huang, L. Qin, J. Wang, X. Zhang, B. Peng, Y. Yu
Department of Materials Science and State Key Laboratory of Molecular Engineering of Polymers
Fudan University
220 Handan Road, Shanghai 200433, China
E-mail: ylyu@fudan.edu.cn

The ORCID identification number(s) for the author(s) of this article can be found under https://doi.org/10.1002/adfm.202208312.

DOI: 10.1002/adfm.202208312

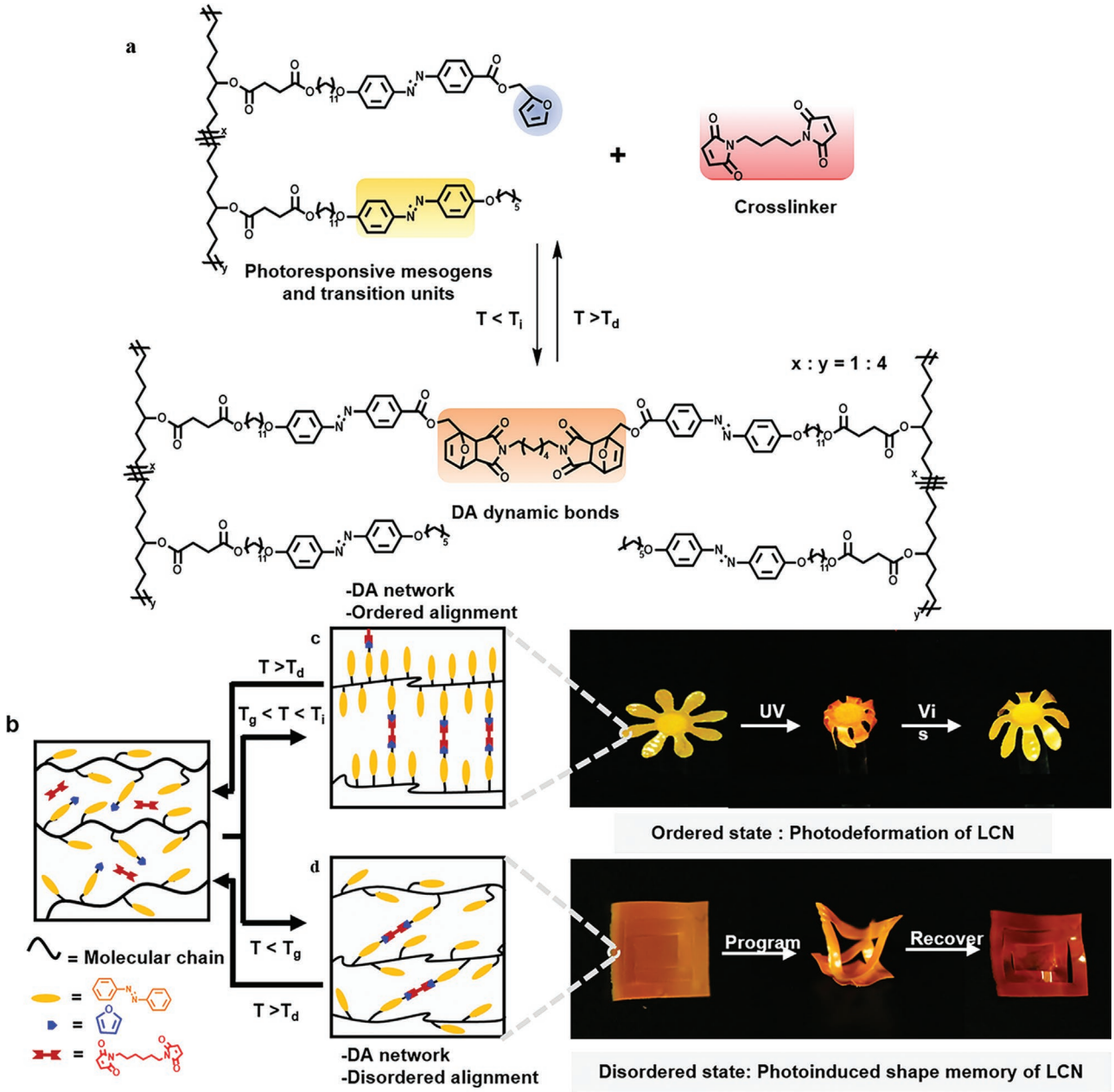

Figure 1. a) The schematic diagram to show the DA reaction ($T < T_i$) of the mixture containing LLCP and crosslinker and the retro-DA reaction ($T > T_d$) of the AZO-DAN. The molecular structures of the azobenzene, furan, crosslinker 1,6-bis (maleimido) hexane, and dynamic Diels-Alder network (AZO-DAN) are marked in yellow, blue, red, and orange, respectively. b) Schematic illustration to show the mixtures of LLCP and crosslinker. c) Schematic illustration to show the AZO-DAN with ordered mesogen alignment (Ordered state) and photographs to show the photodeformation. d) Schematic illustration to show the AZO-DAN with disordered mesogen alignment (Disordered state) and photographs to show the light-induced shape memory performance. T_i, isotropic temperature; T_d, disassociation temperature of DA bonds.

of UV light, reducing the $T_{g\text{-cis}}$ below RT to release the stored entropic energy. However, no remarkable photodeformation is observed in such LCN with ester bonds due to the disordered mesogens alignment, because the T_v of transesterification (180 °C) is much higher than the T_i (95 °C) of the LCN.

Herein, we integrate the multiple shape manipulation of a novel LCN containing both azobenzene moieties and dynamic DA network (AZO-DAN), including reversible photodeformation, light-induced shape memory effect, and shape remolding (**Figure 1**a). The AZO-DAN is obtained after the formation of the DA network with the mixture of linear liquid crystal polymer (LLCP) and crosslinker (Figure 1a, which can be regained by heating the AZO-DAN above the disassociation temperature (T_d) of DA bonds. After annealing at the temperature (T) between the T_g and the T_i, the mesogens self-assemble into an ordered alignment in the presence of the DA network (referred to as the ordered state), and the AZO-DAN generates reversible deformation upon photoisomerization of azobenzene

(Figure 1b,c). When T is below the T_g, due to the weak segment mobility that hinders self-assembly, the mesogens are aligned randomly during the formation of the DA network (referred to as the disordered state), contributing to light-induced shape memory performance (Figure 1b,d). Moreover, the AZO-DAN is remolded to diverse 3D origami and kirigami structures based on the solid state plasticity due to dynamic equilibrium of the DA network. Further, the AZO-DAN is recycled by heating above T_d (Figure 1c,b; Figure 1d,b), exhibiting liquid state remoldability endowed by the disassociation of DA bonds.

2. Results and Discussion

We designed a novel LLCP consisting of azobenzene and furan moieties, which was further cross-linked with 1,6-bis(maleimido)hexane (BMI) to prepare the AZO-DAN by cycloaddition reaction (Figure 1a). Azobenzene moieties in the side chains act as both photoresponsive mesogens and light-switchable transition units. The DA network formed by furan moieties and BMI is employed to lock the mesogen alignment and undergo the topological rearrangement by exchange DA reaction. The flexible backbone and long spacer provide enough free volume for the mesogens to self-assemble into an ordered LC phase. The mixture of the LLCP and BMI is annealed at the temperature between the T_g and the T_i of the LLCP to obtain ordered mesogen alignment. In this scenario, the azobenzene mesogens self-assemble into a lamellar structure that is simultaneously locked by the formed DA network, whose photodeformation is attributed to the order-disorder phase transition (Figure 1b,c; ordered state). In contrast, if the mixture of the LLCP and BMI is cross-linked at the temperature below the T_g, the azobenzene mesogens will be randomly aligned since the weak segment mobility hinders self-assembly of the mesogens. Therefore, this disordered AZO-DAN possesses light-induced shape memory effect with the aid of light-switchable T_g (Figure 1b,d; disordered state).

The LLCP with high molecular weight was synthesized by the ring-opening metathesis polymerization, which was then mixed with a stoichiometric quantity of BMI in tetrahydrofuran (THF) and cast on the glass substrate (please see Figures S1–S4, Supporting Information, for the synthetic route). Because the T_g and the T_i of the LLCP recorded by DSC curves were 45 °C and 94 °C respectively (Figure S5, Supporting Information), the resultant film after the evaporation of THF was annealed at 70 °C (T_g < 70 °C < T_i) to obtain the ordered mesogen alignment by self-assembly. The formation of the DA network was confirmed by infrared spectra of the LLCP and the AZO-DAN film, in which the 1775 cm^{-1} peak located at the curve of the AZO-DAN is specific to DA reaction products of BMI and furan moieties (**Figure 2**a). The changes of the absorption bands characterized by UV–vis absorption spectroscopy indicate that the AZO-DAN is able to undergo *trans-cis* photoisomerization in response to UV and visible light (Figure 2b).

The ordered mesogen alignment is the prerequisite for the reversible photodeformation. As Figure 2c shows, the azobenzene mesogens self-assemble into a lamellar structure, which is confirmed by the emergence of two diffraction peaks with q ratio of 1:2 in the 1D small-angle X-ray scattering (1D SAXS) profiles. Moreover, as investigated by 2D X-ray in Figure 2d, the splitted diffractions in both the low- and high-angle regions demonstrate the formation of the smectic phase. In the high-angle region, the two diffraction arcs appear on the equator, which illuminates the formation of smectic A phase (shown by the inset in Figure 2c). When irradiated with UV light, the AZO-DAN film bent away from the light source owing to the expansion of the irradiated side caused by the disruption of SmA through the *trans-cis* isomerization of the azobenzene mesogens. Moreover, the bent film returned to the initial state upon the irradiation of visible light, since the azobenzene mesogens recovered the ordered alignment due to the *cis* to *trans* back isomerization. (Figure 2e; Movie S1, Supporting Information). In addition, the film exhibited stable light-induced bending during 15 cycles without obvious fatigue (Figure S6, Supporting Information). Furthermore, the photo-induced bending angle gradually became larger as the UV light intensity increased from 0 to 50 mW cm^{-2} (Figure S7, Supporting Information).

In order to obtain the disordered state, the mixture of the LLCP and BMI was cross-linked at 30 °C lower than the T_g of the LLCP (45 °C). The disappearance of diffraction arcs in the high-angle region of the 2D XRD pattern and the uniform diffraction ring in the low-angle region indicate that the mesogen alignments are disordered in the obtained AZO-DAN film (**Figure 3**a). The frozen segments of the LLCP at glassy state hinder the self-assembly of the mesogens,[35] and the random alignment is locked by the formed DA network to give rise to the disordered state. After the irradiation of UV light, the T_g of the AZO-DAN is switched from 43 °C of *trans* form to -12 °C of *cis* form (Figure 3b). The *cis*-form AZO-DAN is at rubbery state, whose segments are activated to program the temporary shape at RT, while the *trans*-form AZO-DAN is at glassy state, indicating that the segments are frozen to fix the temporary shape at RT. Due to the dynamic equilibrium of the DA network, complete stress relaxation was confirmed by the dynamic mechanical analysis (DMA) curve at 80 °C for 90 min (Figure 3c), contributing to the shape remolding caused by solid plasticity. Moreover, the higher temperature the faster relaxation, which reveals that the DA bonds exhibit preference for the retro-DA reaction in high temperatures.

Thanks to the solid state plasticity and the liquid state remoldability, light-induced shape memory effect and shape remolding are demonstrated by using the disordered AZO-DAN films. As shown in **Figure 4**a, the permanent shape 1 ($T_{g\text{-trans}}$ above RT, glassy state) was irradiated with UV light and the *trans* form azobenzene moieties isomerized to the *cis* form, resulting in the $T_{g\text{-cis}}$ of the AZO-DAN below RT. Therefore, the permanent shape 1 was programmed into the temporary shape under external stress. Next, the temporary shape was fixed after the subsequent irradiation with visible light to induce *cis-trans* back isomerization. Shape recovery of the permanent shape 1 was triggered by the irradiation of UV light, reducing the $T_{g\text{-cis}}$ below RT to release the stored entropic energy (Figure 4b; Movie S2, Supporting Information). Subsequently, the permanent shape 1 was plastically deformed (80 °C, 100 min) to a drastically different permanent shape 2 (the kirigami structure) on account of the topological rearrangement of the DA network, which further underwent another shape memory cycle

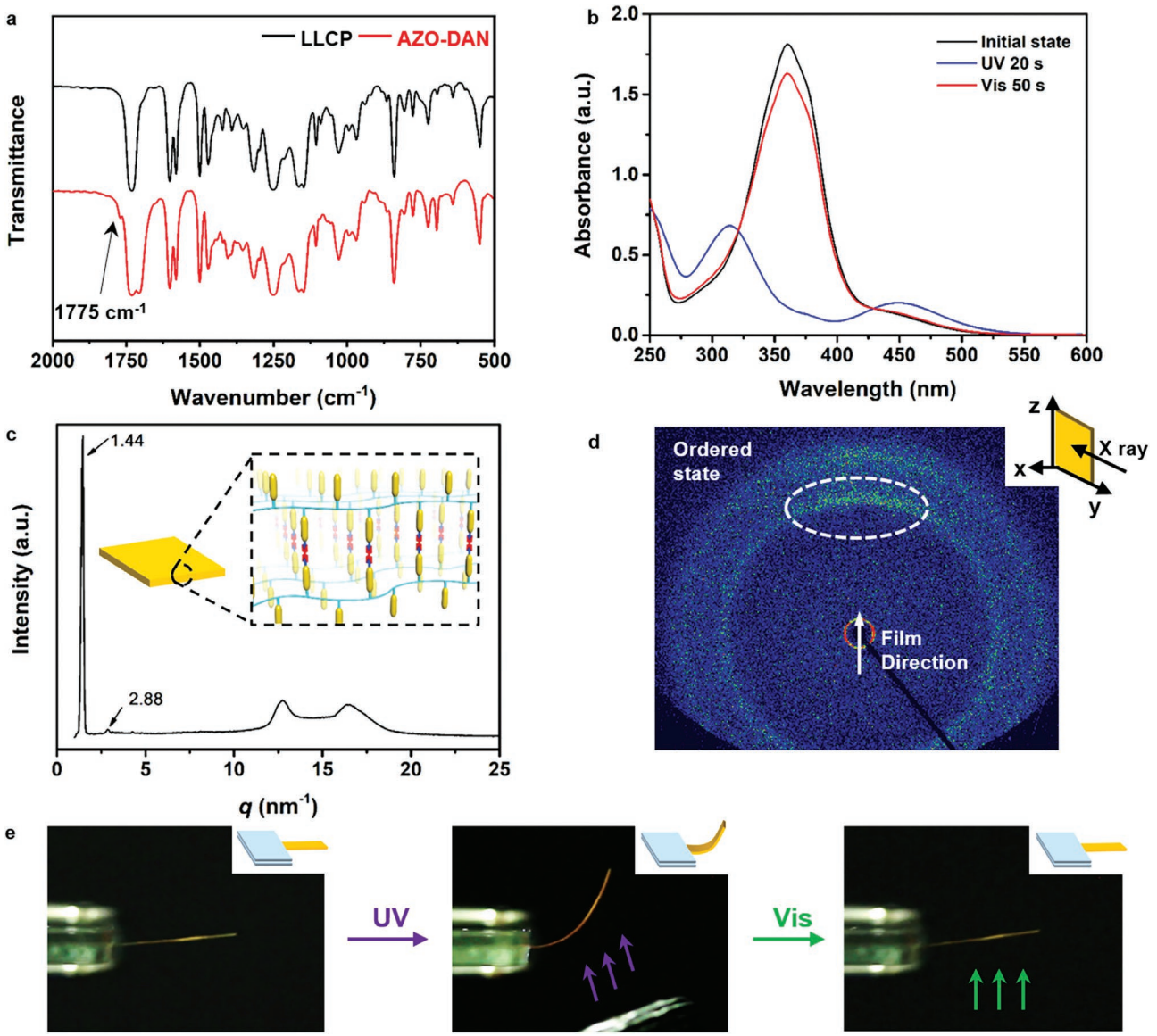

Figure 2. a) FT-IR spectra of the LLCP and the AZO-DAN film. b) UV–vis absorption spectra of the AZO-DAN film before irradiation, after UV irradiation (365 nm, 40 mW cm^{-2}, and 20 s), and subsequent visible-light irradiation (530 nm, 30 mW cm^{-2}, 50 s). c) 1D SAXS spectrum of the AZO-DAN film (ordered state) at room temperature. Inset, schematic illustration to show the SmA phase structure. d) 2D XRD pattern of the AZO-DAN film (ordered state) at room temperature. The X-ray beam is perpendicular to the film direction. e) Photographs to show the bending and unbending of the AZO-DAN film (ordered state, 20 mm × 5 mm × 0.03 mm) under irradiation with UV light (365 nm, 40 mW cm^{-2}) and visible light (530 nm, 30 mW cm^{-2}), respectively. Purple and green arrows indicate the irradiation direction of UV and visible light, respectively.

(Figure 4c; Movie S3, Supporting Information). At a higher temperature of 130 °C, the permanent shape 2 was remolded into a fiber actuator while maintaining its excellent shape memory characteristics, resulting from the dynamic equilibrium of the DA network that shifts to bond breaking direction with increasing temperature (Figure 4d; Movie S4, Supporting Information).

We measured the DSC curves of the AZO-DAN and the LLCP and the TGA curve of the AZO-DAN, confirming that the DA bonds disassociate in the temperature range from 110 to 130 °C. When heated above the disassociation temperature of the DA bonds, the AZO-DAN possessed similar processing capacity as linear polymers, which were able to be processed by solution or melting methods (Figure S8, Supporting Information). Furthermore, the light intensity is the key parameter impacting the shape memory behavior. With the intensity of UV light increasing from 10 to 50 mW cm^{-2}, both the fixity ratio and the recovery ratio of disordered AZO-DAN film increased at first (from 10 to 50 mW cm^{-2}) and then inclined to be stable (from 40 to 50 mW cm^{-2}), which exhibited highest values of 93% and 87%, respectively (Figures S9, Supporting Information). Considering the influence of the light gradient on the shape memory behavior, the fixity and recovery ratios of disordered AZO-DAN film with different thickness (20–80 µm) were also

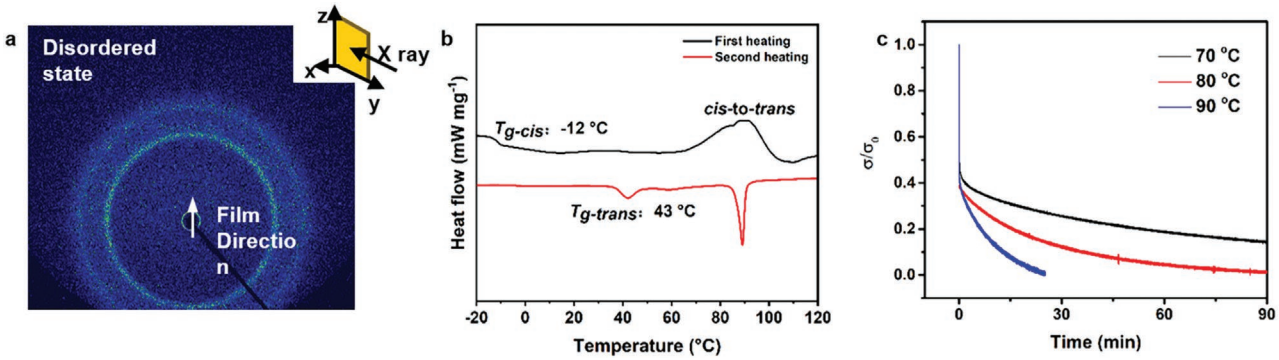

Figure 3. a) 2D-XRD pattern of the AZO-DAN film (disordered state) at room temperature. The X-ray beam is perpendicular to the film direction. b) DSC curves of the *cis*-form AZO-DAN (disordered state) showing the *cis*-glass transition temperature ($T_{g\text{-cis}}$) at –12 °C. The second heating curve shows the *trans*-glass transition temperature ($T_{g\text{-trans}}$) at 43 °C. c) Stress relaxation of the AZO-DAN at different temperatures at a fixed strain of 30%.

investigated, which demonstrated that the thickness had little effect on the shape memory functionality (Figure S10, Supporting Information). In addition, it was worth noting that the temperature of the AZO-DAN only increased by 4 °C under the irradiation of 60 mW cm^{-2} UV light for 2 min; therefore, such a weak photothermal effect during the light-induced shape morphing process was not enough to induce the rearrangement of the topology network of the AZO-DAN (Figure S11, Supporting Information).

AZO-DAN with different alignment states provides selectable light-driven building blocks to assemble the photoresponsive soft actuators with diverse shapes and deformation modes. We used the different AZO-DAN films to fabricate a butterfly (ordered state) and a flower (disordered state) as shown in **Figure 5**a (Movie S5, Supporting Information). First, the opened flower irradiated with UV light was programmed to the closed state by external force, which was then fixed with visible light. Then the closed petals underwent precise shape recovery from close to open state individually with the directed irradiation of UV light, mimicking the blooming of flowers in nature (Figure 5b). Subsequently, we put the butterfly (ordered state) on the blooming flower, and the reversible flapping of the wing was realized when the wing of butterfly was irradiated with UV light and visible light alternatively (Figure 5c).

3. Conclusion

In summary, we reported a novel strategy to integrate reversible photodeformation, light-induced shape memory effect, and shape remolding into the LCN containing both azobenzene moieties and dynamic DA network. Azobenzene moieties act as both photoresponsive mesogens in reversible photodeformation and light-switchable transition unit in shape memory effect. Moreover, benefitting from the dynamic equilibrium of the DA network, the AZO-DAN actuators with diverse 3D geometric shapes were reprogrammed by melt and solution processing methods, including origami structure, kirigami structure, and fiber. The liquid state remoldability and solid state plasticity represent two mechanisms to manipulate the permanent shape during the shape memory performance. It is worth mentioning that the alternative performance of reversible photodeformation and light-induced shape memory effect is determined by the ordered or disordered states in the AZO-DAN actuators, which has the same molecular structure but different mesogen alignments. The mesogens self-assembled into the ordered SmA phase when AZO-DAN was annealed at the temperatures between T_g and T_i, whereas the mesogens were aligned randomly at the temperatures below T_g. Furthermore, AZO-DAN with different alignment states was used as light-driven building blocks to imitate the opening of "shape memory flower" and the flapping of "photodeformable butterfly wings". We believe that the combination of this novel polymer with advanced processing methods such as 3D printing will promote the development of the LCNs and provide tremendous potentials for the design of all-optical soft actuators.

4. Experimental Section

Materials: 4-Aminobenzoic acid (Adamas, 98%), phenol (Greagent, ≥99%), 11-bromo-1-undecanol (Adamas, 99%), furfuryl alcohol (Adamas, 99%), 1-(3-dimethylaminopropyl)-3-ethylcarbodiimide hydrochloride (EDC) (Adamas, 97%), 4-dimethylaminopyridine (DMAP) (Adamas, 99%), 1,5-cyclooctadiene (TCI, 98%), Grubb's second generation catalyst (Aldrich, 98%), and *N*,*N*-hexamethylenebismaleimide (TCI, 97%) were used. Other solvents and reagents used in this study were purchased from Adamas-beat, J&K Scientific, and Sigma–Aldrich. All chemicals were purchased commercially and used as-received. Synthesis and characterization of the LLCP are described in the Supporting Information.

Synthesis of AZO-DAN Film with Disordered State: LLCP of 50 mg was dissolved in 1.5 mL of tetrahydrofuran and the mixture mixed with 1,6-Bis(maleimido) hexane with the furan/maleimide molar ratio of 1:1.1. The mixture was dropped onto a glass substrate. After the solvent was evaporated at room temperature, the film was placed at 30 °C for 48 h to obtain a disordered AZO-DAN film.

Synthesis of AZO-DAN Film with Ordered State: The mixture was prepared according to the same method described above and dripped onto a glass substrate. After the evaporation of the solvent at 70 °C for 4 h, an AZO-DAN film with ordered state was obtained.

Characterization Methods: ^{1}H NMR spectra of the LLCP were recorded on a Bruker DMX500 NMR spectrometer using tetramethylsilane as the internal standard and $CDCl_3$ as the solvent. FT-IR spectra of AZO-DAN were recorded on a Nicolet Nexus 470 spectrometer. The molecular weight as well as the polydispersity index were measured by gel permeation chromatography (GPC, Shimazu, LC-10ADvp) with

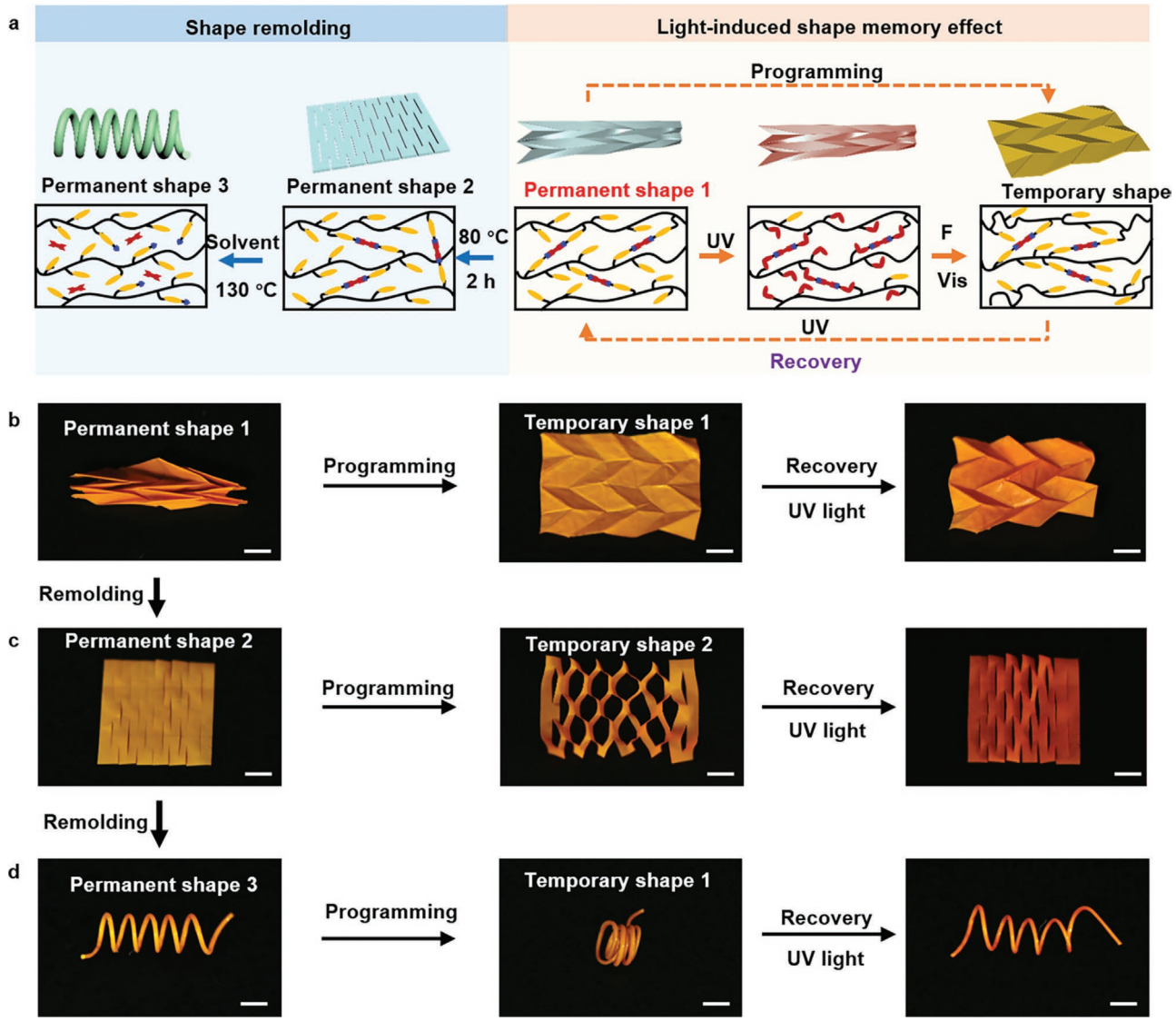

Figure 4. a) Schematic illustration to show the light-induced shape memory effect and the shape remolding of the AZO-DAN sample (disordered state). b) Photographs to show the shape memory performance of the AZO-DAN sample (size 3 cm × 2 cm × 0.05 mm) with the origami structure. c) Photographs to show the shape memory performance of the on-demand remolding of kirigami structure of the AZO-DAN sample (size 2 cm × 2 cm × 0.05 mm). d) Photographs to show the shape memory performance of the on-demand remolding of the AZO-DAN fiber (diameter 100 µm). Scale bars: 0.5 cm. Permanent shape 1, origami structure; permanent shape 2, kirigami structure; permanent shape 3, and fiber.

tetramethylsilane as the solvent at a flow rate of 5 mL min^{-1}. The thermodynamic properties of LLCP and AZO-DAN were determined by DSC (TA, Q2000) at a heating and cooling rate of 10 °C min^{-1}. The textures of LLCP and AZO-DAN were evaluated with a POM (Leika, DM2500p) equipped with a hot stage (Linkam THMS600). 1D SAXS measurements were carried out on a Bruker NanoSTAR SAXS system using Cu Kα (λ = 1.542 Å) as the radiation source. 2D XRD experiments were conducted on a small-angle/wide-angle diffractometer (Xeuss 2.0) with a 2D detector of Pilatus3R in transmission mode. UV–vis absorption spectra were measured with a UV–vis absorption spectrophotometer (HITACHI, U-4100). Photographs and videos of the deformation behaviors were taken by a super-resolution digital microscope (Keyence, VHX-1000C). The 365 nm UV light was generated by an Omron ZUV-H30MC light source with a ZUV-C30H controller. 530-nm visible light was generated by a CCS HLV-24GR-3 W.

The Molding of Permanent Shape 1: First, the flat AZO-DAN film was manually folded into origami structure. Then, it was placed in an oven at T = 80 °C for 3 h with external force that was applied to retain its origami structure. After that, the folded film was removed from the heat source and cooled to room temperature, obtaining permanent shape 1.

The Molding of Permanent Shape 2: The film in permanent shape 1 was unfolded and then placed in an oven at T = 80 °C for 2 h with external force applied to retain its flat state. Afterward, the flat film was cut according to a designed route, obtaining permanent shape 2.

The Molding of Permanent Shape 3: The film in permanent shape 2 was heated to 130 °C for 15 min, breaking up the Diels–Alder bonds. Then the melt was remolded into a spiral fiber through melting drawing spinning, and obtaining permanent shape 3.

Shape Memory Cycle: First, the film in a permanent shape was irradiated with UV light (40 mW cm^{-2}) for 30 s, and then manually stretched. When an external force was applied for shape retaining, the film was irradiated with visible light (50 mW cm^{-2}) for 5 min in order to fixing the temporary shape. Finally, the film recovered to its original state after irradiated with UV light (40 mW cm^{-2}) for 30 s.

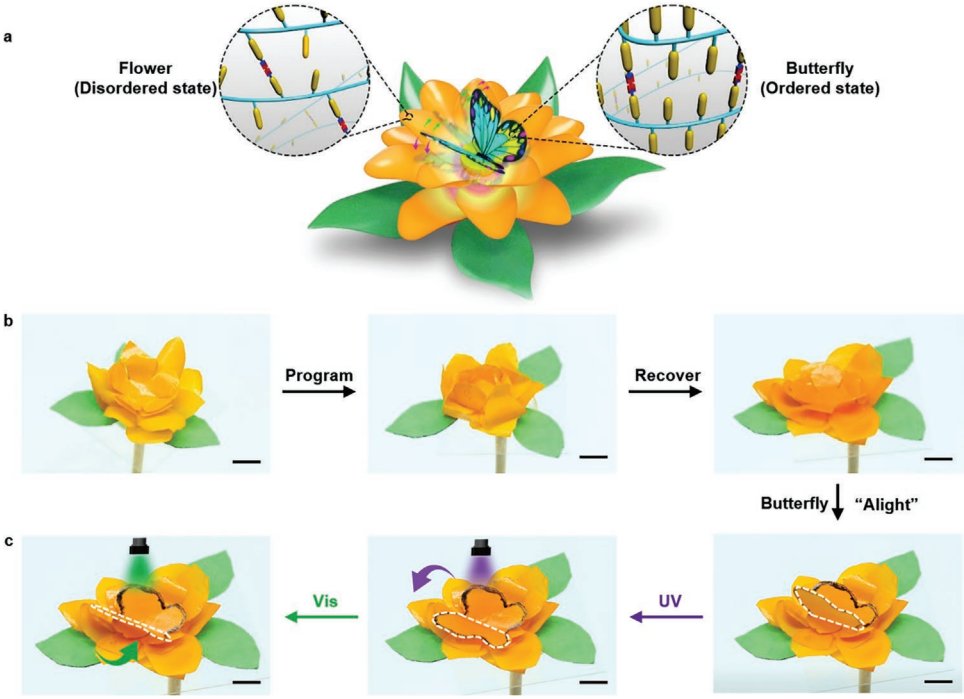

Figure 5. a) Schematic illustration to show the flower and butterfly prepared by the AZO-DAN films with different states. Butterfly, ordered state; flower, disordered state. b) Photographs to show the closure and opening of the flower (disordered state) by light-induced shape memory effect (365 nm, 40 mW cm^{-2}, 530 nm, and 30 mW cm^{-2}). c) Photographs to show reversible wing flapping of the butterfly (ordered state) by photodeformation (365 nm, 40 mW cm^{-2}, 530 nm, and 30 mW cm^{-2}). Purple arrows indicate the bending direction of the irradiated wing, green arrows indicate the direction of wing's recovery. Scale bar: 0.5 cm.

Supporting Information

Supporting Information is available from the Wiley Online Library or from the author.

Acknowledgements

This work was supported financially from the National Natural Science Foundation of China (21734003 and 51927805), and Innovation Program of Shanghai Municipal Education Commission (2017-01-07-00-07-E00027).

Conflict of Interest

The authors declare no conflict of interest.

Data Availability Statement

The data that support the findings of this study are available from the corresponding author upon reasonable request.

Keywords

dynamic networks, liquid crystal polymers, photodeformation, shape memory effect

Received: July 20, 2022
Revised: September 11, 2022
Published online:

[1] Q. Zhao, W. Zou, Y. Luo, T. Xie, *Sci. Adv.* **2016**, *2*, 1501297.
[2] X. Pang, J. Lv, C. Zhu, L. Qin, Y. Yu, *Adv. Mater.* **2019**, *31*, 1904224.
[3] J. Sun, B. Peng, Y. Lu, X. Zhang, J. Wei, C. Zhu, Y. Yu, *Small* **2021**, *18*, 2106443.
[4] Y. Chen, Q. Liu, P. Theato, J. Wei, Y. Yu, *Adv. Intell. Syst.* **2021**, *3*, 2000254.
[5] Q. Ze, X. Kuang, S. Wu, J. Wong, S. M. Montgomery, R. Zhang, J. M. Kovitz, F. Yang, H. J. Qi, R. Zhao, *Adv. Mater.* **2020**, *32*, 1906657.
[6] H. Finkelmann, E. Nishikawa, G. G. Pereira, M. Warner, *Phys. Rev. Lett.* **2001**, *87*, 015501.
[7] X. Pang, L. Qin, B. Xu, Q. Liu, Y. Yu, *Adv. Funct. Mater.* **2020**, *30*, 2002451.
[8] T. Ikeda, M. Nakano, Y. Yu, O. Tsutsumi, A. Kanazawa, *Adv. Mater.* **2003**, *15*, 201.
[9] Y. Yu, M. Nakano, T. Ikeda, *Nature* **2003**, *425*, 145.
[10] C. L. van Oosten, C. W. Bastiaansen, D. J. Broer, *Nat. Mater.* **2009**, *8*, 677.
[11] H. Li, Q. Liu, C. Zhu, J. Wei, Y. Yu, *Liq. Cryst.* **2020**, *47*, 1154.
[12] S. Han, Y. Chen, B. Xu, J. Wei, Y. Yu, *Chin. J. Polym. Sci.* **2020**, *38*, 806.
[13] S. Iamsaard, S. J. Asshoff, B. Matt, T. Kudernac, J. J. L. M. Cornelissen, S. P. Fletcher, N. Katsonis, *Nat. Chem.* **2014**, *6*, 229.
[14] S. V. Ahir, A. R. Tajbakhsh, E. M. Terentjev, *Adv. Funct. Mater.* **2006**, *16*, 556.
[15] M. H. Li, P. Keller, B. Li, X. Wang, M. Brunet, *Adv. Mater.* **2003**, *15*, 569.
[16] F. Zhai, Y. Feng, Z. Li, Y. Xie, J. Ge, H. Wang, W. Qiu, W. Feng, *Matter* **2021**, *4*, 3313.
[17] W. Zou, X. Lin, E. M. Terentjev, *Adv. Mater.* **2021**, *33*, 2101955.
[18] Z. Pei, Y. Yang, Q. Chen, E. M. Terentjev, Y. Wei, Y. Ji, *Nat. Mater.* **2014**, *13*, 36.

[19] Y. Xia, G. Cedillo-Servin, R. D. Kamien, S. Yang, *Adv. Mater.* **2016**, *28*, 9637.
[20] H. Lu, M. Wang, S. Huang, X. Chen, Z. Liu, H. Yang, *Acta Polym. Sin.* **2021**, *52*, 304.
[21] T. H. Ware, M. E. McConney, J. J. Wie, V. P. Tondiglia, T. J. White, *Science* **2015**, *347*, 982.
[22] M. Fang, T. Liu, Y. Xu, B. Jin, N. Zheng, Q. Zhao, Z. Jia, T. Xie, *Adv. Mater.* **2021**, *33*, 2105597.
[23] B. Buguin, M. H. Li, P. Silberzan, B. Ladoux, P. Keller, *J. Am. Chem. Soc.* **2006**, *128*, 1088.
[24] C. M. Spillmann, J. Naciri, B. R. Ratna, R. L. B. Selinger, J. V. Selinger, *J. Phys. Chem. B* **2016**, *120*, 6368.
[25] Y. Xiao, Z. Jiang, X. Tong, Y. Zhao, *Adv. Mater.* **2019**, *31*, 1903452.
[26] K. M. Lee, M. L. Smith, H. Koerner, N. Tabiryan, R. A. Vaia, T. J. Bunning, T. J. White, *Adv. Funct. Mater.* **2011**, *21*, 2913.
[27] M. Wang, Z. Cheng, B. Zuo, X. Chen, S. Huang, H. Yang, *ACS Macro Lett.* **2020**, *9*, 860.
[28] D. Montarnal, M. Capelot, F. Tournilhac, *Science* **2011**, *334*, 965.
[29] T. Ube, K. Kawasaki, T. Ikeda, *Adv. Mater.* **2016**, *28*, 8212.
[30] X. Lu, S. Guo, X. Tong, H. Xia, Y. Zhao, *Adv. Mater.* **2017**, *29*, 1606467.
[31] M. K. Mcbride, A. M. Martinez, L. Cox, M. Alim, K. Childress, M. Beiswinger, M. Podgorski, B. T. Worrell, J. Killgore, C. N. Bowman, *Sci. Adv.* **2018**, *4*, eaat4634.
[32] M. K. McBride, M. Hendrikx, D. Liu, B. T. Worrell, D. J. Broer, C. N. Bowman, *Adv. Mater.* **2017**, *29*, 1606509.
[33] G. Zhang, Q. Zhao, L. Yang, W. Zou, X. Xi, T. Xie, *ACS Macro Lett.* **2016**, *5*, 805.
[34] Z. Jiang, Y. Xiao, L. Yin, L. Han, Y. Zhao, *Angew. Chem., Int. Ed.* **2020**, *16*, 4925.
[35] T. Xie, *Polymer* **2011**, *52*, 4895.
[36] X. Zhang, C. Zhu, B. Xu, L. Qin, J. Wei, Y. Yu, *ACS Appl. Mater. Interfaces* **2019**, *11*, 46212.